



1                                    **Bardsey – an island in a strong tidal stream**  
2                                    **Underestimating coastal tides due to unresolved topography**

3

4                                    **J. A. Mattias Green<sup>1,\*</sup> and David T. Pugh<sup>2</sup>**

5

6                                    <sup>1</sup> School of Ocean Sciences, Bangor University, Menai Bridge, UK

7                                    <sup>2</sup> National Oceanography Centre, Joseph Proudman Building, Liverpool, UK

8                                    \* Corresponding author: Dr Mattias Green, m.green@bangor.ac.uk

9

10

11

12                                    **Abstract**

13                                    Bardsey Island is located at the western end of the Llŷn Peninsula in north-west Wales Separated from  
14                                    the mainland by a channel some 3 km wide, it is surrounded by reversing tidal streams of up to 4 ms<sup>-1</sup>  
15                                    <sup>1</sup> at spring tides. These local hydrodynamic details and their consequences are unresolved by satellite  
16                                    altimetry, nor are they represented in regional tidal models. Here we look at the effects of the island  
17                                    in the strong tidal stream in terms of the formation and shedding of eddies, and the budgets for tidal  
18                                    energy dissipation. We show, using local observation and a satellite altimetry constrained product,  
19                                    that the island has a large impact on the tidal stream, and that even the latest altimetry database  
20                                    seriously under-represents the tidal stream due to the island not being resolved. The effect of the  
21                                    island leads to an underestimate of the current speed in the altimetry data in the channel of up to a  
22                                    factor of three, depending on tidal state, and the average tidal energy resource is underestimated by  
23                                    a factor 6. The observed tidal amplitudes are higher at the mainland than at the island, and there is a  
24                                    detectable phase lag in the tide across the island – this effect is not seen in the altimetry data. The  
25                                    underestimate of the tide in the altimetry data has consequences for tidal dissipation and wake effect  
26                                    computation and show that local observations are key to correctly estimate tidal energetics around  
27                                    small-scale coastal topography.

28



## 29 1 Introduction

30 Scientific understanding of global tidal dynamics is well established. Following the advent of satellite  
31 observations, several tidal constituents can be mapped from altimetry data, and the products  
32 constrained using in situ tidal databases (e.g., TPXO - Egbert and Erofeeva, 2002 and  
33 [http://volkov.oce.orst.edu/tides/tpxo9\\_atlas.html](http://volkov.oce.orst.edu/tides/tpxo9_atlas.html), and FES - [https://www.aviso.altimetry.fr](https://www.aviso.altimetry.fr/en/data/products/auxiliary-products/global-tide-fes.html)  
34 [/en/data/products/auxiliary-products/global-tide-fes.html](https://www.aviso.altimetry.fr/en/data/products/auxiliary-products/global-tide-fes.html)). There is, however, still an issue in terms  
35 of spatial resolution of the altimetry products: even the most recent tidal models have only  $1/30^\circ$   
36 resolution (equivalent to  $\sim 3.2$  km in longitude at the equator, some 1.9 km in the domain here, and  
37 3.2 km in latitude everywhere). This means that smaller topographic features and islands are  
38 unresolved, and may be “invisible” to the altimetry product even if the features may be resolved in  
39 the latest bathymetry databases, e.g., GEBCO (<https://www.gebco.net/>). Consequently, local tidal  
40 dynamics, for example wake effects behind an island or headland, are poorly represented. Here, we  
41 use a series of tide-gauge measurements from Bardsey Island in the Irish Sea (Figure 1) to evaluate  
42 the effect of the island on the tidal dynamics as they track around Bardsey Island and the Llŷn  
43 peninsula in North Wales, UK.

44  
45 Bardsey Island, which we use for this study, is a rocky melange of sedimentary and igneous rocks  
46 including some granites, located 3.1 km off the Llŷn Peninsula in North Wales (Figure 1a). It is  
47 approximately 1 km wide, though only 300 m at the narrowest part, and 1.6 km long. It reaches 167  
48 m at its highest point. Bardsey Sound, between the Llŷn peninsula and the island, experiences strong  
49 tidal currents. The relatively small scale of the island and the separating Sound means that the local  
50 detail is not “seen” in the altimetry products: this will lead to effects induced by the island being  
51 missed in the altimetry data. The uncaptured (by TPXO) very active local tidal dynamics allows us to  
52 compare altimetry constrained tidal characteristics, especially amplitudes, for the region with  
53 accurate local observations, and quantify the validity limits of the altimetry products. We will do a  
54 direct comparison of tidal amplitudes around the island (see Figure 1b for TG locations and a summary  
55 of the in-situ tides). We also consider whether, and when, in the tidal cycle, flow separation occurs in  
56 the wake of the island.

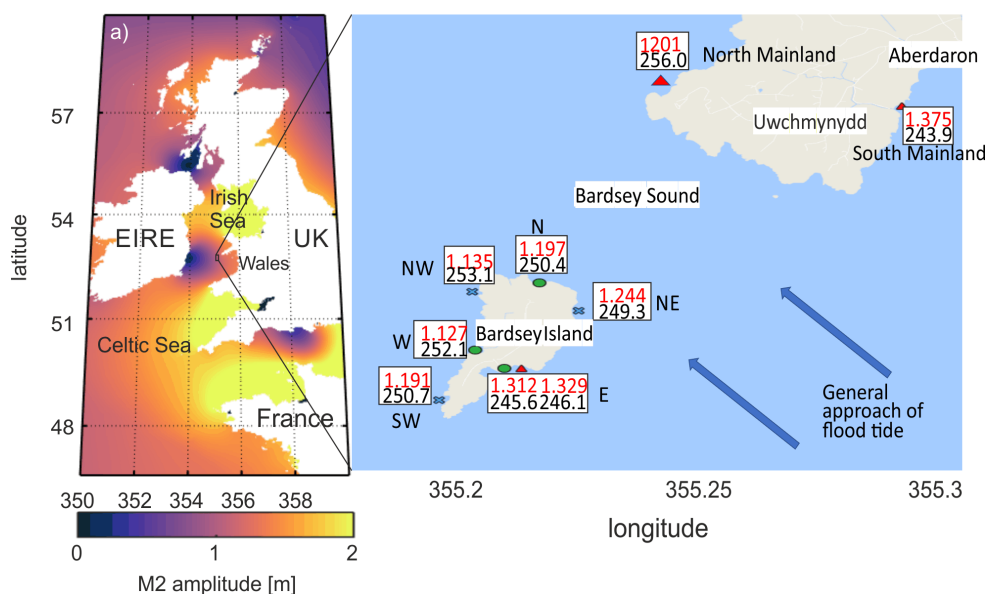
57  
58 We will use some basic fluid-flow parameters. Transition to turbulence can be parameterised in terms  
59 of the Reynolds number,  $Re$ , defined as  $Re = UD/\nu$ , where  $U$  is a velocity scale,  $D$  is the size of the  
60 object, and  $\nu \sim 100$  is the kinematic viscosity (Edwards et al., 2004; Wolanski et al., 1984). It indicates  
61 when the transition to turbulence occurs: at low Reynolds numbers,  $Re < 1$ , the flow is quite symmetric  
62 upstream and downstream, and there is no flow separation at the object. As the Reynolds number is  
63 increased to the range  $10 < Re < 40$ , laminar separation happens and results in two steady vortices  
64 downstream. As  $Re$  increases further, up to  $Re < 1000$ , these steady vortices are replaced by a periodic  
65 von Karman vortex street, whereas if  $Re > 1000$ , the separated flow is fully turbulent.

66  
67 Another useful non-dimensional number for this type of investigation is the Strouhal number,  $St =$   
68  $fD/U$ . Here,  $f$  is the frequency of the shedding of vortices, and fully developed vortices are generated  
69 when  $T > f$  and  $T$  is the frequency of the oscillating flow (Dong et al., 2007; Magaldi et al., 2008). If,  
70 on the other hand, the tidal frequency is larger than  $f$  only one wake eddy will be shed on each tidal cycle,  
71 if it has time to form at all.

72



73



74

75 Figure 1: a) Map of the European shelf showing  $M_2$  tidal amplitudes in meters, from TPX09. b) details  
76 of local topography and tidal characteristics in the vicinity of Bardsey Island. The symbols mark the TG  
77 location, with green ellipses denoting phase 1, blue crosses phase 2, and red triangles phase 3.  
78 Note that East was occupied twice, during Phases 1 and 3. The red numbers in the text boxes are the  
79 amplitudes (in meters) and the phases (in degrees, one degree is two minutes in time) from the  
80 harmonic analysis for each tide gauge. Map data ©Google Earth.

81

82

## 83 2 Observations

### 84 2.1 In situ data collection

85 The tidal elevations around Bardsey were measured in three phases, from summer 2017 through to  
86 spring 2018 (Table 1 and Figure 1b). Note that site East, the main Harbour for the island, Y Cafn, was  
87 occupied twice as a control, during Phase 1 and 3, and that all the other instrument deployments were  
88 bottom mounted a few tens of metres offshore in depths between 3.2 to 16.5 m. The instruments  
89 used were RBR pressure recorders with a measurement resolution better than 0.001 m. The  
90 instruments were set to sample every 6 minutes, and the resulting pressure series were subjected to  
91 harmonic analysis using the NOC TASK software (details are available from  
92 [https://www.psmsl.org/train\\_and\\_info/software/task2k.php](https://www.psmsl.org/train_and_info/software/task2k.php)).

93

94 Analyses were made for 26 constituents, including Mean Sea Level and eight related constituents,  
95 appropriate for a month or more of data (see, e. g., Pugh and Woodworth, 2014). The non-tidal  
96 residuals have standard deviations appropriate for the region at the times of year of the deployments.  
97 Phase 2 residuals, however, are noticeably higher than the other two phases because it included one  
98 of the most severe storms and waves in local memory: hurricane Ophelia. A good indication of the



99 quality of the in-situ observations and analyses is given by the consistency in the tidal ages and  $S_2/M_2$   
 100 amplitude ratios in the final column of Table 2.

101

102 Table 1: Details of the pressure gauge deployments. Amplitudes are given to three decimal places as  
 103 appropriate for the uncertainties, whereas the timing of constituent phases is probably better than  
 104 0.5 degrees (1 minutes for  $M_2$ ).

105

Station	Latitude	Longitude	Deployed	Recovered	Depth mean (m)	Non-tidal Standard deviation (m)
Phase 1						
North	52.767	355.213	1605 25/5/17	1400 11/7/17	3.9	0.113
East	52.756	355.207	1557 25/5/17	1350 3/7/17	7.0	0.141
West	52.753	355.202	1045 27/5/17	1128 5/7/17	5.6	0.116
Phase 2						
Northwest	52.765	355.203	0000/ 1/9/17	1110 27/10/17	6.7	0.156
Southwest	52.748	355.197	0000/ 1/9/17	1145 30/10/17	7.5	0.154
Northeast	52.762	355.220	0000/ 1/9/17	1240 30/10/17	5.5	0.150
Phase 3						
East	52.753	355.207	1512 7/09/18	0912 05/10/18	3.2	0.095
South Mainland	52.759	355.275	1348 7/09/18	1024 06/10/18	4.8	0.088
North Mainland	52.781	355.236	1500 7/09/18	1512 10/10/18	16.5	0.083

106

107

## 108 2.2 Altimetry data

109 The altimetry data came from the TPX09 ATLAS ([http://volkov.oce.orst.edu/tides/tpxo9\\_atlas.html](http://volkov.oce.orst.edu/tides/tpxo9_atlas.html);  
 110 (Egbert and Erofeeva, 2002). The resolution is  $1/30^\circ$  in both latitude and longitude (3.7 km and 2.2 km  
 111 at Bardsey). We used the elevation and transport information, and their respective phases, for the  $M_2$ ,  
 112  $S_2$ ,  $N_2$ , and  $M_4$  constituents. In the following calculations, we define “astronomical” as the largest  
 113 possible current speed or amplitude, computed as the sum of the amplitudes with the four tidal  
 114 constituents we discuss. This is thus a limited form of Highest and Lowest Astronomical Tide.

115

## 116 2.3 LANDSAT data

117 Landsat-8 data images were used to identify possible eddies in the currents. Data were downloaded  
 118 from the Earth Explorer website (<https://earthexplorer.usgs.gov/>). True colour enhanced RGB images  
 119 were created with SNAP 7.0 using the panchromatic band for red (500 - 680nm, 15m resolution), band  
 120 3 for green (530 - 590nm, 30m resolution) and Band 2 for blue (450 - 510 nm, 30m resolution). The  
 121 blue and green bands were interpolated using a bicubic projection to the 15m panchromatic  
 122 resolution, and brightness was enhanced to allow easier visualization of the wakes. Images were taken  
 123 between 11:00 and 12:00 UTC over the area.

124

125

126



127 **3 Results**

128

129 Table 2 Summary of harmonic tidal analyses. TPX09 data interpolated to the TG location, which are  
 130 given in **BOLD**. “H” is amplitude (in m) and “G” is phase (degrees relative to Greenwich, given in italics  
 131 to ease reading). TGX09 amplitudes are given to 0.01 m, whereas the *in situ* precision justifies  
 132 resolution to 0.001 m.

		M2		S2		M4		Tidal Age (hours)	M2/S2 ratio
		TG	TPXO	TG	TPXO	TG	TPXO		
<b>PHASE 1</b>									
North	H	<b>1.197</b>	1.17	<b>0.458</b>	0.45	<b>0.112</b>	0.12		<b>0.383</b>
	G	<b>250.4</b>	254.4	<b>287.1</b>	287.3	<b>20.5</b>	32.4	<b>36.7</b>	
East	H	<b>1.312</b>	1.16	<b>0.514</b>	0.42	<b>0.144</b>	0.12		<b>0.392</b>
	G	<b>245.6</b>	253.8	<b>283.4</b>	286.7	<b>45.8</b>	34.3	<b>37.8</b>	
West	H	<b>1.127</b>	1.15	<b>0.434</b>	0.42	<b>0.136</b>	0.12		<b>0.385</b>
	G	<b>252.1</b>	253.7	<b>288.4</b>	286.6	<b>34.9</b>	34.8	<b>36.3</b>	
<b>PHASE 2</b>									
NW	H	<b>1.135</b>	1.16	<b>0.431</b>	0.4215	<b>0.130</b>	0.12		<b>0.380</b>
	G	<b>253.1</b>	254.7	<b>287.1</b>	287.6	<b>35.0</b>	33.4	<b>34.0</b>	
SW	H	<b>1.191</b>	1.15	<b>0.461</b>	0.42	<b>0.088</b>	0.12		<b>0.387</b>
	G	<b>250.7</b>	253.4	<b>285.5</b>	286.3	<b>26.0</b>	35.6	<b>34.8</b>	
NE	H	<b>1.244</b>	1.5	<b>0.482</b>	0.43	<b>0.094</b>	0.12		<b>0.387</b>
	G	<b>249.3</b>	253.8	<b>284.0</b>	286.7	<b>42.6</b>	32.8	<b>34.7</b>	
<b>PHASE 3</b>									
East	H	<b>1.329</b>	1.16	<b>0.522</b>	0.42	<b>0.136</b>	0.12		<b>0.393</b>
	G	<b>246.1</b>	253.8	<b>282.8</b>	286.7	<b>53.2</b>	34.3	<b>36.7</b>	
S. Mainland	H	<b>1.375</b>	1.21	<b>0.538</b>	0.44	<b>0.149</b>	0.14		<b>0.391</b>
	G	<b>243.9</b>	251.5	<b>280.7</b>	284.4	<b>49.9</b>	37.1	<b>36.8</b>	
N. Mainland	H	<b>1.201</b>	1.20	<b>0.461</b>	0.43	<b>0.072</b>	0.12		<b>0.384</b>
	G	<b>256.0</b>	254.6	<b>290.4</b>	287.6	<b>39.0</b>	29.1	<b>34.4</b>	

133

134

135 **3.1 Amplitudes and phases**

136 A spring-neap cycle of parts of the data from the East and West gauges in phase 1 is plotted in Figure  
 137 2. The TG data show amplitudes of 1.197 m (North), 1.312 m (east) and 1.127 m (west). These give  
 138 across-island difference in amplitude of about -14% (on spring tides a level difference across 300 m of  
 139 up to 0.3 m), and an along-island difference of about -9% (compared to the data from the Eastern TG).  
 140 There is also 6.5° (13 minutes) phase difference for M<sub>2</sub> across the island between the east and the  
 141 west, with the east leading, consistent with the tide approaching the island from the south and east  
 142 and then swinging up around the Llyn Peninsula headland (see Figures 2b,c and 3). This curvature of  
 143 the streamlines as the flow is squeezed through Bardsey Sound and swings up around the peninsula,  
 144 leads to the enhanced generation of non-linear higher tidal harmonics due to curvature on the



145 reversing tidal stream curves. This contributes to the large  $M_4$  amplitudes around the island and  
146 headland (Table 2).

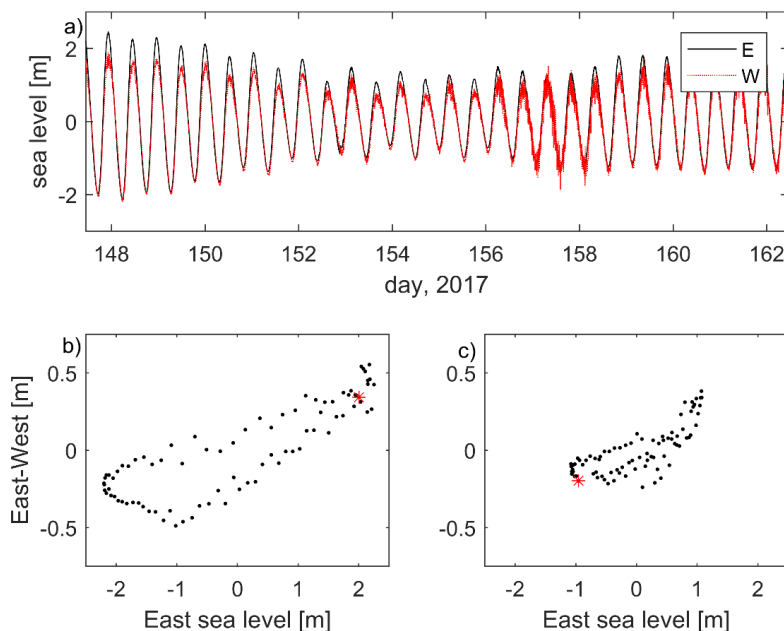
147

148 In contrast, the TPXO9  $M_2$  data, which has no island representation, if interpolated linearly to the TG  
149 positions, come out as 1.17, 1.16, and 1.15 m for the phase 1 locations (Table 2). The corresponding  
150 TPXO-phases are  $254.4^\circ$ ,  $253.8^\circ$ , and  $253.7^\circ$ , indicating that there is only a small variation in the tidal  
151 signal (2cm in amplitude and  $0.7^\circ$  in phase) over the location of the island in the altimetry data. The  
152 results in Table 2 show that there is a substantial effect of the island and limited resolution, inducing  
153 a 13% change in amplitude between the TPXO and TG data at station East. These results are supported  
154 by the phase 2 measurements (Table 2). Phase 3 saw an extended and different approach to the data  
155 collection. We revisited East, but also deployed two gauges on the Llŷn peninsula, on the approach to  
156 the island (South Mainland)), and north of it (North Mainland). At South Mainland, TPXO is again  
157 underestimating the tidal amplitude by more than 10%. At North Mainland, some 5 km north of  
158 Bardsey, and just north of the Sound, however, the TG and TPXO amplitudes are within 1 cm of each  
159 other. This again shows the effect Bardsey and local topography, have on the tidal amplitudes in the  
160 region.

161

162 For the shallow-water tidal harmonics, the TPXO  $M_4$  amplitude agrees well with the TG data at North  
163 (0.12 and 0.11 m, respectively), but overestimates the amplitude at North Mainland (0.07 m in the TG  
164 data and 0.12 m from TPXO; see Table 2). Because higher harmonics are generated locally by the tidal  
165 flow itself, this again shows the effect of the island on the tidal stream; the  $M_4$  amplitude is halved  
166 along Bardsey Sound in the TG data, whereas TPXO overestimates it and shows only minor variability.  
167 The overestimate in TPXO can lead to the tidal energetics being biased high in the region if they are  
168 based on the altimetry alone.

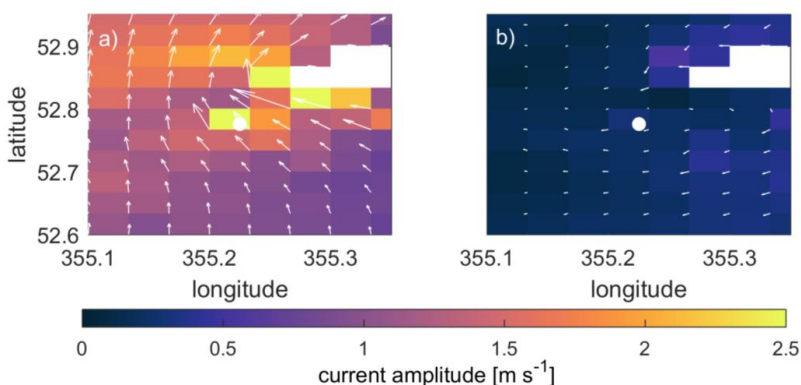
169



170



171 Figure 2: a: Part of the East (black) and West (red) data series from Phase 1, covering one spring-neap  
 172 cycle (arbitrary datums).  
 173 b and c: plots of the elevation at East vs. the East-West difference in elevation for springs (b, day 147)  
 174 and neaps (c, day 154). The red stars show the first data point of the day. The progression is clockwise.  
 175  
 176  
 177 3.2 Currents



178  
 179 Figure 3: The current magnitude (colour) and vectors at neap ebb (a) and spring flood (b) from TPXO9.  
 180 The white circle shows the location of Bardsey – note that it is not resolved in the TPXO data base and  
 181 has been added for visual purposes only.

182  
 183 We do not have access to any current measurements from the region, but the tidal stream is known  
 184 to reach up to  $4 \text{ m s}^{-1}$  in the Sound (Colin Evans, pers. comm. and Admiralty chart no. 1971). The TPXO9  
 185 spring flood and neap flood currents are shown in Figure 3. It is reasonable to assume that, to first  
 186 order, the acceleration into the Sound can be described as a frictionless Bernoulli flow driven by the  
 187 sea-surface elevation change between South and north Mainland (e.g., Stigebrandt, 1980),

$$0.5u^2 = g\Delta H \quad (1),$$

188  
 189  
 190  
 191 where  $u$  is the speed in the Sound, and  $\Delta H$  is the associated drop in sea-surface elevation (the water  
 192 column depth changes little between South Mainland and North Mainland and the depth difference  
 193 is thus neglected). We can add the speed at South mainland,  $u_{SM}$ , to Eq. (1) to get the total speed in  
 194 the strait. Using data for M2 from TPXO9 gives a 0.01 m change in tidal amplitude along the Sound,  
 195 which when used in Eq. (1) gives a current speed, induced by the sea-level difference, of  $0.4 \text{ m s}^{-1}$   
 196 between South Mainland and North Mainland. If we add the TPXO9 M<sub>2</sub> speed at South Mainland,  $u_{SM}$   
 197 =  $1 \text{ m s}^{-1}$ , to this we get  $u_{M2}=1.4 \text{ m s}^{-1}$  at North Mainland from TPXO9. The actual TPXO9 speed at the  
 198 position of the North Mainland TG is  $u_{M2} = 1.3 \text{ m s}^{-1}$ , and the calculation implies that TPXO  
 199 underestimates the currents in the Sound. The same computation from the astronomic tide  
 200 differences gives  $u_{astro} = 2.7 \text{ m s}^{-1}$ , using  $\Delta H=0.07\text{m}$  and  $u_{astro, SM}= 1.5 \text{ ms}^{-1}$ , which is a serious  
 201 underestimate compared to the suggested astronomic tide of  $4 \text{ m s}^{-1}$ . However, the phases are ignored  
 202 here, and the instantaneous gradient along the sound is larger – for M2 the phase difference equates



203 to 13 minutes, so the instantaneous gradient can be up to 11% larger and the resulting flow can thus  
204 be up to 23% stronger, or  $1.7 \text{ m s}^{-1}$ .

205

206 If, on the other hand, we take the TPXO speed at South Mainland as true, because it is not as  
207 influenced by the presence of the island as North Mainland, and repeat the calculations using the  
208 observed changes in amplitudes from the TG data, the 0.16 m drop between South Mainland and  
209 North Mainland in the  $M_2$  tidal amplitudes gives  $2.8 \text{ m s}^{-1}$  in the Sound from  $M_2$  alone (or  $3.4 \text{ m s}^{-1}$  if  
210 we include a correction for the phase). The astronomic difference (e.g., using all constituents) between  
211 South and North Mainland is 33 cm, giving  $2.5 \text{ m s}^{-1}$  from the TG difference, which when added to the  
212 South Mainland  $u_{\text{astro,SM}} = 1.5 \text{ m s}^{-1}$ , gives  $4 \text{ m s}^{-1}$  at North Mainland – in agreement with the estimates  
213 of local sea-going experts, and the Admiralty chart for the Sound.

214

215

### 216 3.3 Dissipation

217 In the computations above we neglected friction, which is probably a crude approximation. To first  
218 order, dissipation can be computed from the (adjusted) TPXO velocities and from the observed  
219 amplitude drop along the Sound by comparing the tidal energy flux,  $E_f$ , between the two locations. A  
220 decrease in the energy flux between two locations can be associated with local dissipation of tidal  
221 energy as the wave propagates them (see e.g., Green et al., 2008). The flux of tidal energy is given by  
222 (e.g., Phillips, 1977)

223

$$224 E_f = 0.5c_g\rho gH^2 \quad (3),$$

225

226 where  $H$  is again the tidal amplitude and  $c_g = \sqrt{gh}$  is the speed of the tidal wave ( $h$  is the water  
227 depth). The dissipation,  $\varepsilon$ , is then the difference in energy flux between the two mainland TG locations,  
228 or  $\varepsilon = c_g\rho g(H_{SM}^2 - H_{NM}^2)$ , taking  $c_g$  constant because  $h$  changes little between the TG locations. Using  
229 the TG amplitudes, the astronomic tide would then dissipate  $243 \text{ kW m}^{-1}$ . Over the 3.1 km width of  
230 the Sound, this integrates to about 750 MW. The  $M_2$  tide contributes 26% of this, or 201 MW. This is  
231 approximately 0.1% of the total  $M_2$  dissipation on the European shelf estimated from large-scale  
232 altimetry (Egbert and Ray, 2000), and is a reasonable estimate for such an energetic region. Note that  
233 this method is independent of the phases between the locations, nor does it depend on the phases  
234 between the amplitudes and currents.

235

236 If these calculations are repeated using the TPXO elevations, the astronomic dissipation comes out as  
237 126 MW and the  $M_2$  dissipation as 11 MW. This is a substantial underestimate (factors of almost 6 and  
238 more than 18, for the astronomic and  $M_2$  tides, respectively), which again highlights the importance  
239 of resolving small-scale topography in local tidal energy estimates, and the use of direct observations  
240 in coastal areas to constrain any modelling effort. This dissipation occurs only a small fraction of the  
241 European Shelf and coastline, and although the Bardsey tides are unusually energetic, underestimated  
242 local coastal energy dissipation may be substantial in satellite altimetry data and numerical models.

243

### 244 3.4 Caveat Emptor!

245 We have shown above that the tidal elevations are underestimated in the altimetry data, and that the  
246 current magnitude is most likely underestimated as well, so our computations below are conservative.





247 The two extremes in tidal current magnitude in Bardsey Sound can be taken to be the neap tide speed  
248 from TPXO9 and the astronomic speed computed using TG data and TPXO combined. We thus have  
249  $0.9 \text{ m s}^{-1}$  (neaps from TPXO9, not discussed above) as the lower range, and  $4 \text{ m s}^{-1}$  (astronomic  
250 computed) as the upper estimate.

251

252 Even using the much-underestimated current speeds from the TPXO-data, the indications are that  
253 there would be no stratification locally. The Simpson-Hunter parameter,  $X = h/u^3 \approx 70$  for Bardsey  
254 Sound (Simpson and Hunter, 1974). This means that the area is vertically mixed due to the tides alone.  
255 The eddies shed from the island will add more energy to this, further breaking down any potential  
256 stratification from freshwater additions (the Simpson-Hunter parameter is based on heat fluxes only)  
257 and act to redistribute sediment. The associated Reynolds number for the Island,  $Re=UD/\nu$ , then  
258 comes out at approximately 10 for the neap flow, or approximately 40 for the astronomic tidal current  
259 (using  $D=1000 \text{ m}$  as the width and  $\nu=100 \text{ m}^2 \text{ s}^{-1}$  as the eddy viscosity). This implies laminar separation  
260 into two steady vortices downstream of the Island at peak flows, and the vortices can be expected to  
261 appear on both ebb and flood flows (Edwards et al., 2004; Wolanski et al., 1984). There may not be  
262 any vortex shedding during neap flows, however, because  $Re \sim 10$ .

263

264 The Strouhal number  $St = fL/U$ , is typically about 0.2 for the  $Re$  numbers found here (Wolanski et al.,  
265 1984), giving  $f=St U/L = 0.2U/1500 \Rightarrow 1 \times 10^{-4} < f < 5 \times 10^{-4}$  and an associated vortex shedding period of  
266 3-17 hours ( $L=1500 \text{ m}$  is the length of the island). This means that fully developed eddies, generated  
267 at the higher flow rates, because our tidal period (12.4 hours) is longer than the vortex shedding period  
268 (semi-diurnal vs. a few hours), whereas at neap flows, there is no time to develop a fully separated  
269 vortex in a tidal cycle.

270



271

272 Figure 4: Landsat 8 images from October 5, 2017 (a) and September 13, 2018 (b) from Landsat 8. The  
273 tidal phase are halfway between neaps and springs in a) and just after spring high tide in b). The white  
274 dot north of the island in Figure 3b is an exposed rock generating a second wake. See  
275 <https://landsat.gsfc.nasa.gov/data/> for data availability.

276

277 This conclusion is supported by satellite images from Landsat 8 (Figure 4), which shows a very different  
278 picture between neaps (Figure 3a) and springs (Figure 4b). At spring tides, there are two clear wakes



279 behind the tips of the island (marked with arrows), whereas at neaps (Figure 4a) there is only a more  
280 diffuse image in Bardsey Sound, and no signal of a wake behind the south tip of the island.

281

282

#### 283 4 Discussion

284 This brief account was triggered by an interest in detailed mapping of tides in a reversing tidal stream.  
285 The results highlight the effect small coastal islands can have on tides in energetic settings, and they  
286 highlight the limitations of altimetry-constrained databases near coastlines where the bathymetry is  
287 unresolved. Even though TPX09, which is used here, is constrained by a series of tide gauges in the  
288 Irish Sea, including north and south of Bardsey, the island is some 60 km from the nearest long-term  
289 tide gauge (in Holyhead, some 45 km to the north of Bardsey). Consequently, the tidal amplitudes in  
290 the database are not representative of the observed amplitudes near the island, and the currents are  
291 underestimated by a factor close to 1.5 for the astronomic tide. This underestimate also means that  
292 wake effects may be underestimated if one relies solely on altimetry (or coarse resolution numerical  
293 models) unable to resolve islands, with consequences for navigation, renewable energy installations,  
294 and sediment dynamics.

295

296 The results do have wider implications for, among others, the renewable industry, because we show  
297 that local observations are necessary in regions of complex geometry to ensure the energy resource  
298 is determined accurately. Using only TPX0 data, the dissipation – an indicator of the renewable  
299 resource – is underestimating the astronomic potential with a factor 6 of the real resource. There is  
300 also the possibility that wake effects behind the island would be neglected without proper surveys,  
301 leading to an erroneous energy estimate. The results also highlight that concurrent sea-level and  
302 current measurements are needed to fully explore the dynamics and quantify, e.g., further pressure  
303 effects of the island on the tidal stream. Consequently, we argue that in any near-coastal investigation  
304 of detailed tidal dynamics, the coastal topography must be explicitly resolved, and any modelling  
305 effort should be constrained to fit local observations of the tidal dynamics.

306

307

308 **Acknowledgements:** Instrument deployments and recovery were planned and executed with the  
309 assistance of the Bardsey ferry operator, Colin Evans, and by Ernest Evans, the local lobster fisherman  
310 and expert on Bardsey tidal conditions. The Phase 1 observations were partly funded by the Crown  
311 Estate. The Landsat data was processed by Dr Madjid Hadjal and Professor David McKee at University  
312 of Strathclyde.

313

314 **Code/Data availability:** The data is available from the Open Science Framework  
315 ([https://osf.io/kvgur/?view\\_only=ff2d8bd12a61493aa1dfa9011ecdde81](https://osf.io/kvgur/?view_only=ff2d8bd12a61493aa1dfa9011ecdde81))

316

317 **Author contributions:** JAMG wrote the manuscript and did the computations. DTP did the  
318 measurements, processed the TG data, and assisted with the writing.

319

320 **Competing interests:** The authors declare no competing interest

321

322



323 References

- 324 Dong, C., McWilliams, J. C. and Shchepetkin, A. F.: Island Wakes in Deep Water, *J. Phys. Oceanogr.*,  
325 37(4), 962–981, doi:10.1175/jpo3047.1, 2007.
- 326 Edwards, K. A., MacCready, P., Moum, J. N., Pawlak, G., Klymak, J. M. and Perlin, A.: Form Drag and  
327 Mixing Due to Tidal Flow past a Sharp Point, *J. Phys. Oceanogr.*, 34(6), 1297–1312,  
328 doi:10.1175/1520-0485(2004)034<1297:fdamdt>2.0.co;2, 2004.
- 329 Egbert, G. D. and Erofeeva, S. Y.: Efficient inverse Modeling of barotropic ocean tides, *J. Atmos.*  
330 *Ocean. Technol.*, 19, 183–204, 2002.
- 331 Egbert, G. D. and Ray, R. D.: Significant dissipation of tidal energy in the deep ocean inferred from  
332 satellite altimeter data, *Nature*, 405(6788), 775–778, doi:10.1038/35015531, 2000.
- 333 Green, J. A. M., Simpson, J. H., Legg, S. and Palmer, M. R.: Internal waves, baroclinic energy fluxes  
334 and mixing at the European shelf edge, *Cont. Shelf Res.*, 28(7), 937–950,  
335 doi:10.1016/j.csr.2008.01.014, 2008.
- 336 Magaldi, M. G., Özgökmen, T. M., Griffa, A., Chassignet, E. P., Iskandarani, M. and Peters, H.:  
337 Turbulent flow regimes behind a coastal cape in a stratified and rotating environment, *Ocean*  
338 *Model.*, 25(1–2), 65–82, doi:10.1016/J.OCEMOD.2008.06.006, 2008.
- 339 Phillips, O. M.: *The Dynamics of the Upper Ocean*, Cambridge University Press, Cambridge, UK.,  
340 1977.
- 341 Simpson, J. H. and Hunter, J. R.: Fronts in the Irish Sea, *Nature*, 250(5465), 404–406,  
342 doi:10.1038/250404a0, 1974.
- 343 Stigebrandt, A.: Some aspects of tidal interaction with fjord constrictions, *Estuar. Coast. Mar. Sci.*, 11,  
344 151–166, 1980.
- 345 Wolanski, E., Imberger, J. and Heron, M. L.: Island wakes in shallow coastal waters, *J. Geophys. Res.*,  
346 89(C6), 10553, doi:10.1029/jc089ic06p10553, 1984.
- 347